THE JOURNAL OF PHYSICAL CHEMISTRY C

Article

pubs.acs.org/JPCC

A Structural Model for a Self-Assembled Nanotube Provides Insight into Its Exciton Dynamics

Min Gao,[†,§,∥] Subhradip Paul,[†,§,¶] Charles D. Schwieters,[‡] Zhi-Qiang You,[†] Hui Shao,[†,#] John M. Herbert,*[,†] Jon R. Parquette,*[,†] and Christopher P. Jaroniec*[,†]

[†]Department of Chemistry and Biochemistry, The Ohio State University, Columbus, Ohio 43210, United States

[‡]Division of Computational Bioscience, Center for Information Technology, National Institutes of Health, Bethesda, Maryland 20892, United States

Supporting Information

ABSTRACT: The design and synthesis of functional self-assembled nanostructures is frequently an empirical process fraught with critical knowledge gaps about atomic-level structure in these noncovalent systems. Here, we report a structural model for a semiconductor nanotube formed via the self-assembly of naphthalenediimide-lysine (NDI-Lys) building blocks determined using experimental $^{13}C-^{13}C$ and $^{13}C-^{15}N$ distance restraints from solid-state nuclear magnetic resonance supplemented by electron microscopy and X-ray powder diffraction data. The structural model reveals a two-dimensional-crystal-like architecture of stacked monolayer rings each containing ~50 NDI-Lys molecules, with significant π-stacking interactions occurring both within the confines of the ring and along the long axis of the tube. Excited-state delocalization and energy transfer are simulated for the nanotube based on time-dependent density functional theory and an incoherent hopping model. Remarkably, these calculations reveal efficient energy migration from the excitonic bright state, which is in agreement with the rapid energy transfer within NDI-Lys nanotubes observed previously using fluorescence spectroscopy.

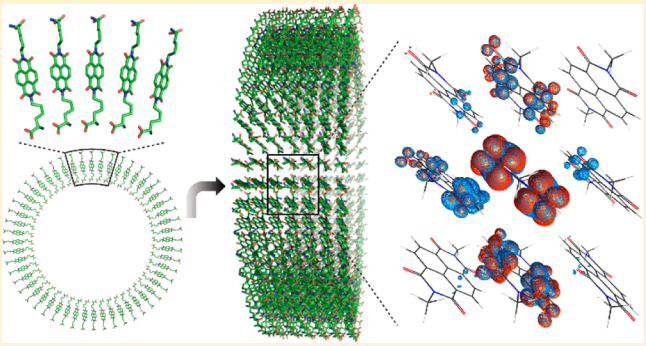

INTRODUCTION

The promise of nano- and mesoscale science to create optoelectronic materials with desired properties, optimal performance, and multifunctionality depends on the ability to modulate the short- and long-range organization of the functional component building blocks.[1−3] The confinement of electronic behavior within such architectures produces a wide range of properties that often differ drastically from the bulk macroscale,[4−6] and novel phenomena are expected to emerge if the collective interactions that comprise these materials can be systematically tuned; the latter remains an elusive synthetic objective.[7,8] Intermolecular effects critically impact the transport of electronic excitation energy through networks of chromophores that transiently store this energy via short-lived excited states.[9] In particular, ordered molecular aggregates often display coherent, cooperative properties that impart onto these systems the ability to delocalize excitations and transport energy and charge over several molecules.[10,11] A prime example of how nature creates such properties is the noncovalent assembly of light-harvesting complexes of bacteriochlorophyll (BChl) in cyclic arrays that engage in extensive *J*-type $\pi-\pi$ stacking interactions.[12] These interactions mediate the delocalization of photoinduced excitons over multiple BChl molecules in the array, which allows each BChl chromophore in the ring to undergo ring-to-ring energy transfer with equal probability, thereby increasing the efficiency of energy harvesting for use in the photosynthetic reaction center.[12,13]

Molecular self-assembly, which can generate complex nanoscale structures by noncovalently packing subunits based on their shape and surface properties,[14,15] provides a viable approach to replicate these types of cyclic chromophore arrays and create the extensive molecular overlap required to propagate excitation energy in materials needed for technologies in nanoscience and optoelectronics.[16,17] However, predictably assembling such superstructures with the specific dimensional resolution necessary to produce a desired property is exceptionally challenging and often discovered empirically.[14] In the absence of precise synthetic methods, a rational design strategy must therefore integrate synthesis with molecular-level structural characterization, both experimental and theoretical, to optimize performance. However, the lack of long-range lattice order coupled with molecular level polymorphism and sample heterogeneity, typical for many noncovalent materials, render the precise determination of molecular packing within self-assembled nanostructures an exceptionally challenging and seldom achieved task.[18,19]

Received: April 8, 2015
Revised: May 20, 2015
Published: May 26, 2015

DOI: 10.1021/acs.jpcc.5b03398
J. Phys. Chem. C 2015, 119, 13948−13956

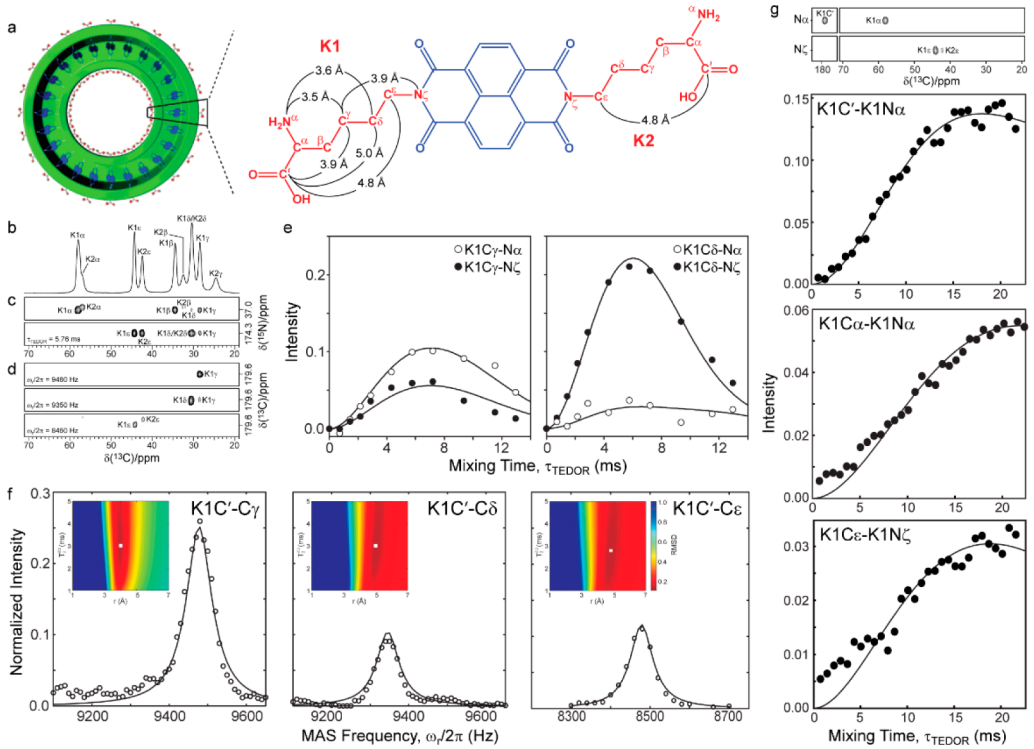

Figure 1. Determination of structural restraints in NDI-Lys nanotubes by MAS solid-state NMR spectroscopy. (a) (Left) Cartoon representation of a monolayer ring structure formed via the self-assembly in water of multiple NDI-Lys monomers. The nanotubes result from the stacking of multiple rings onto each other.[29] (Right) Structural formula of NDI-Lys with the lysine headgroups (red) located on the inner and outer nanotube surfaces labeled as K1 and K2, respectively, showing the intramolecular $^{13}C-^{15}N$ and $^{13}C-^{13}C$ distances greater than 3 Å determined by ZF-TEDOR and R^2W techniques. The intramolecular $^{13}C-^{15}N$ and $^{13}C-^{13}C$ distances were determined using the diluted nanotube sample to minimize the effects of intermolecular couplings (see Methods section). (b) Aliphatic region of a 1D ^{13}C solid-state NMR spectrum of NDI-Lys nanotubes showing the resonance assignments. (c,d) Small regions of representative ZF-TEDOR (panel c) and R^2W (panel d) spectra. The ZF-TEDOR spectrum in panel c was recorded using a MAS rate of 11111 Hz and TEDOR mixing time, τ_{TEDOR}, of 5.76 ms, and shows correlations involving the K1/K2 Nα and Nζ atoms corresponding to ^{15}N frequencies of 37.0/35.6 and 174.3 ppm, respectively. The R^2W spectra in panel d were recorded at MAS frequencies of 9480, 9350, and 8460 Hz and contain correlations between K1/K2 C′ and Cγ, Cδ, and Cε atoms, respectively. (e,f) Representative measurements of $^{13}C-^{15}N$ (panel e) and $^{13}C-^{13}C$ (panel f) distances with experimental data and simulations shown as circles and lines, respectively. The $^{13}C-^{15}N$ and $^{13}C-^{13}C$ distances were extracted using established approaches as described in the Supporting Information. The insets in panel f show the contour plots of the root-mean-square deviation (RMSD) between experimental and simulated trajectories as a function of the $^{13}C-^{13}C$ distance and zero-quantum relaxation (T_2^{ZQ}) parameters. (g) Determination of intermolecular K1C′−Nα, K1Cα−Nα, and K1Cε−Nζ distances using the mixed nanotube sample (see Methods section). The ZF-TEDOR spectrum (top) recorded with τ_{TEDOR} = 18 ms and 11111 Hz MAS shows that $^{13}C'$, $^{13}C\alpha$, and $^{13}C\varepsilon$ correlations arise exclusively from either $^{15}N\alpha$ or $^{15}N\zeta$. This allows measurements of intermolecular $^{13}C-^{15}N$ couplings using 1D band-selective TEDOR, with experimental and simulated trajectories shown as circles and lines, respectively. A summary of all intramolecular and intermolecular distances determined for the NDI-Lys nanotubes is provided in Table 1.

Solid-state nuclear magnetic resonance (NMR) spectroscopy has advanced significantly as a "bottom-up" technique for deriving structural models of noncovalent molecular aggregates that reveal details of both local structure and intermolecular interactions. While cutting-edge solid-state NMR methods have been widely applied toward the structural and dynamic analysis of large peptide and protein complexes,[20−24] analogous detailed studies of synthetic supramolecular assemblies are relatively rare.[19,25−28] In this work, we report a structural model for self-assembled nanotubes composed of a naphthalenediimide-lysine (NDI-Lys) bolaamphiphile,[29] determined using intra- and intermolecular distances derived from magic-angle spinning (MAS) solid-state NMR spectra supplemented by experimental restraints on the nanotube diameter from transmission electron microscopy (TEM) and NDI chromophore spacing from X-ray powder diffraction (XRD). The model reveals both the conformation of the individual NDI-Lys monomer units as well as their hierarchical assembly within the nanotube structure. The nanotubes possess a two-dimensional (2D)-crystal-like architecture assembled via the stacking of initially formed cyclic monolayer membrane rings with ∼50 NDI-Lys molecules per ring. Theoretical studies to simulate the excited-state delocalization and energy transfer within the nanotubes, applied to a portion of the structural model, indicate strong excitonic couplings (comparable in magnitude to those found for BChl pigments in bacterial light-harvesting complexes[30,31]) along both the nanotube axis and around the ring of NDI-Lys chromophores. Remarkably, these theoretical predictions are consistent with the rapid energy transfer within NDI-Lys nanotubes observed previously using fluorescence spectroscopy techniques.[29]

RESULTS

Determination of Intra- and Intermolecular Distances in NDI-Lys Nanotubes by Solid-State NMR Spectroscopy. Initial studies of NDI-Lys nanotubes by MAS solid-state NMR[29] revealed a high degree of molecular order for the monomer units within the nanotube lattice and yielded site-specific chemical

DOI: 10.1021/acs.jpcc.5b03398
J. Phys. Chem. C 2015, 119, 13948−13956

shift assignments for the lysine headgroups located on the inner and outer surfaces of the nanotube (Figure 1a,b). As described in the Methods section, the intramolecular $^{13}C-^{15}N$ and $^{13}C-^{13}C$ distances for the lysine headgroups were determined for a diluted nanotube sample prepared from a physical mixture of $^{13}C,^{15}N$-enriched and natural abundance NDI-Lys in a 15:85 molar ratio using the z-filtered transferred echo double resonance (ZF-TEDOR)[32] and rotational resonance width (R^2W)[33] techniques, respectively. In panels c and d of Figure 1 we show representative regions of ZF-TEDOR and R^2W spectra, respectively, containing multiple cross-peaks reporting on structurally interesting $^{13}C-^{15}N$ and $^{13}C-^{13}C$ through-space dipolar couplings. The corresponding cross-peak buildup trajectories recorded as a function of the dipolar mixing time (for ZF-TEDOR) or MAS frequency (for R^2W) and used to extract quantitative $^{13}C-^{15}N$ and $^{13}C-^{13}C$ distance estimates are shown in panels e and f of Figure 1, respectively. Altogether, these experiments provided a set of seven intramolecular distances between ~3−5 Å as summarized in Table 1 and Figure 1a. Note that the conformation of the lysine headgroup located on the inner surface of the nanotube (labeled K1) is especially well-defined by the experimental solid-state NMR data via six of the seven distance restraints, while only a single distance between the $^{13}C'$ and $^{13}C\varepsilon$ atoms could be determined for the outer lysine (labeled K2). The inability to obtain additional distances involving the K2 atoms is a consequence of conformational dynamics of the K2 headgroup, which lead to increased transverse nuclear spin relaxation and linebroadening and, consequently, low spectral intensities (Figure 1b).

Table 1. Intramolecular and Intermolecular Distances in NDI-Lys Nanotubes

atoms	distance (Å)
K1Cγ—Nα[a]	3.5 ± 0.5
K1Cγ—Nζ	3.9 ± 0.6
K1Cδ—Nα	3.6 ± 0.5
K1C′—Cγ	3.9 ± 0.2
K1C′—Cδ	5.0 ± 0.2
K1C′—Cε	4.8 ± 0.2
K2C′—Cε	4.8 ± 0.3
K1C′- - -K1Nα[b]	3.7 ± 0.5
K1Cα- - -K1Nα	4.8 ± 0.7
K1Cε- - -K1Nζ	5.0 ± 0.8

[a]Intramolecular $^{13}C-^{15}N$ and $^{13}C-^{13}C$ distances (indicated by a solid line between atoms) were determined using the diluted nanotube sample and ZF-TEDOR and R^2W experiments, respectively. [b]Intermolecular $^{13}C-^{15}N$ distances (indicated by a dashed line between the atoms) were determined using the mixed nanotube sample and band selective TEDOR.

To evaluate the interactions between neighboring NDI-Lys monomers within the nanotube assembly, we probed several types of intermolecular $^{13}C-^{15}N$ dipolar couplings in a mixed nanotube sample generated from a physical mixture of ^{13}C- and ^{15}N-NDI-Lys in a 1:1 molar ratio. In analogy to the intramolecular $^{13}C-^{15}N$ distance measurements discussed above, the intermolecular couplings were detectable only for the relatively rigid inner lysine headgroup and included those between K1C′−Nα, K1Cα−Nα, and K1Cε−Nζ atoms. To facilitate these measurements, we first recorded a 2D $^{15}N-^{13}C$ chemical shift correlation spectrum using the ZF-TEDOR pulse scheme[32] with a relatively long dipolar mixing time (τ_{TEDOR} = 18 ms), which emphasizes long-range intermolecular correlations. This spectrum (Figure 1g) revealed that for each ^{13}C site the correlations arise only from one type of ^{15}N nucleus (either Nα or Nζ), which permitted the evaluation of intermolecular $^{13}C-^{15}N$ distances from a series of 1D ^{13}C spectra recorded as a function of the TEDOR mixing time using the band-selective TEDOR scheme[32] that offers enhanced spectral sensitivity by suppressing one-bond $^{13}C-^{13}C$ J-couplings. The experimental TEDOR trajectories are shown in Figure 1g and were fit to an analytical two-spin model described previously[32] in combination with control experiments that account for the effective ^{13}C transverse relaxation rate and overall amplitude scaling as described elsewhere.[34] Note that the minor deviations between experimental and simulated K1Cα−Nα and K1Cε−Nζ trajectories observed for short mixing times (τ_{TEDOR} < 5 ms) are due to intramolecular one-bond dipolar couplings between the $^{15}N\alpha$ and $^{15}N\zeta$ spins and directly bonded ^{13}C nuclei present at natural abundance; these deviations do not have an appreciable effect on the estimation of the intermolecular couplings of interest. Furthermore, the use of the above fitting procedure, which reports on the shortest intermolecular $^{13}C-^{15}N$ distances that dominate the TEDOR trajectories, is appropriate in the present context given the lack of a priori information about the nanotube structure. The resulting intermolecular distances are summarized in Table 1.

Nanotube Structure and Hierarchical Assembly. NDI-Lys nanotubes have been shown to assemble via the stacking of monolayer rings composed of multiple NDI-Lys bolaamphiphile monomer units.[29] The number of monomers per ring is a critical parameter required for the determination of a global nanotube structural model and was estimated as follows. A series of preliminary structure calculations was performed for nanotubes made up of six rings and containing between 28 and 64 NDI-Lys monomers per ring, subject to intramolecular NMR distances and a restraint on the ring radius based on TEM measurements of the nanotube width (Figure 2f−h). These calculations intentionally excluded the intermolecular K1C′−Nα distance restraint to allow the number of monomers per ring and the spacing between them to be systematically varied. For each structure, the XRD pattern was calculated using the debyer program (http://code.google.com/p/debyer) as described in the Supporting Information. The calculated XRD patterns (Figure S1b of the Supporting Information) reveal a strong correlation between the position of a major diffraction peak and the spacing between adjacent NDI-Lys monomers within the ring (Figure S1c). Comparison of the location of this peak with the corresponding feature in the experimental XRD pattern for NDI-Lys nanotubes[29] (Figure 2e) indicates that the nanotubes contain on the order of 48−64 monomers per ring (c.f., Figure S1 caption). To further narrow this range and provide a single best estimate for the number of NDI-Lys molecules per ring for the final nanotube structure calculations, we also inspected the magnitudes of the intramolecular distance and van der Waals energy terms for each of the calculated structures (Figure S1d). The relatively large increases in both of these energy terms observed upon increasing the number of monomers per ring from 52 to 56 suggest that nanotubes containing 52 NDI-Lys molecules per ring are most consistent with the experimental NMR and XRD data and yield structural models with acceptable van der Waals repulsion energies, with the caveat that some variability in the exact number of monomers per ring is to be naturally expected within individual NDI-Lys nanotubes in a macroscopic sample in spite

DOI: 10.1021/acs.jpcc.5b03398
J. Phys. Chem. C 2015, 119, 13948−13956

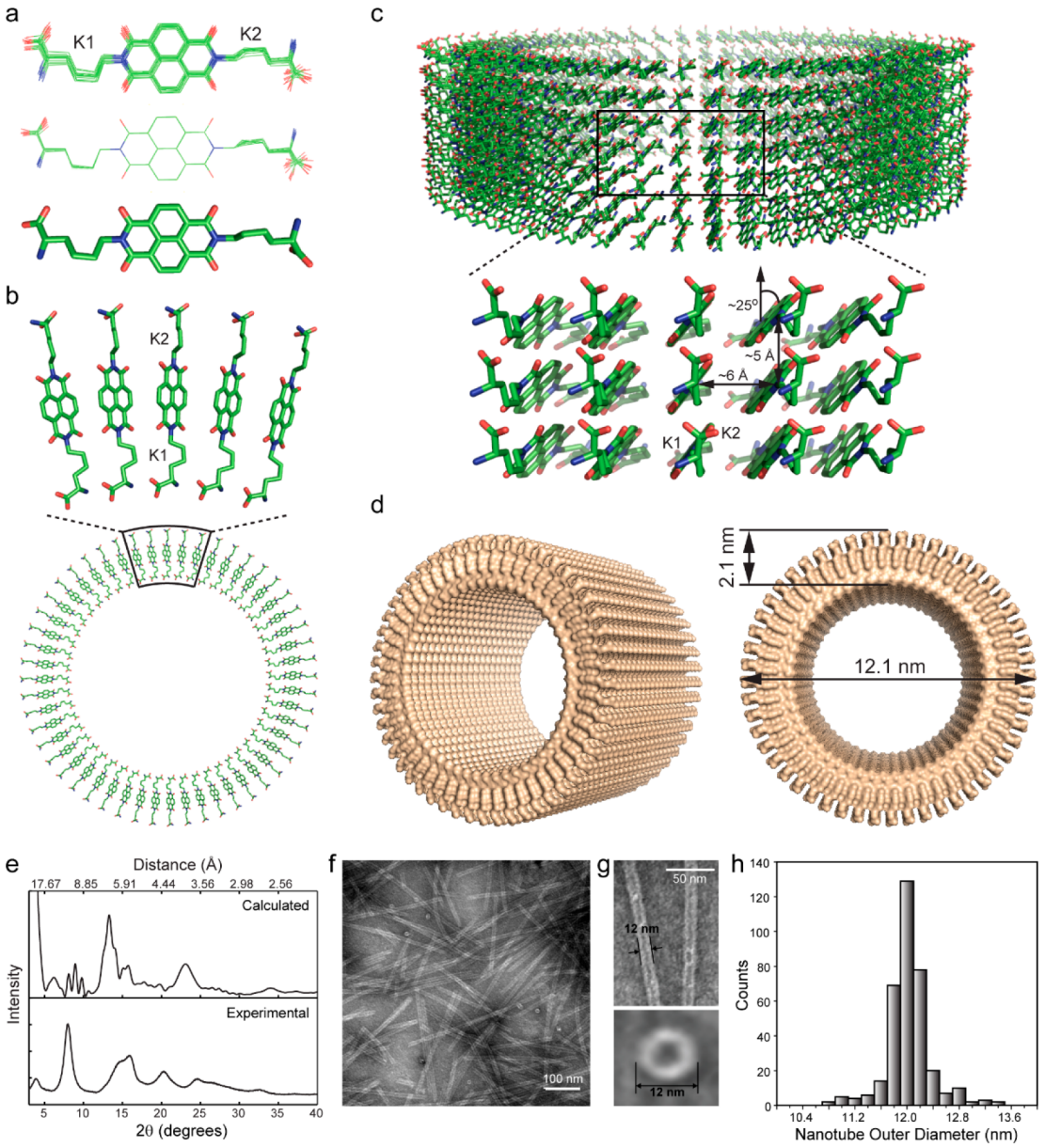

Figure 2. Structure and hierarchical assembly of NDI-Lys nanotubes. (a) (Top) Twenty lowest-energy structures for a representative NDI-Lys monomer extracted from the structural model of the corresponding nanotube containing seven rings with 52 monomers per ring (cf., Figure S2 in the Supporting Information). As described in the Methods section, a total of 200 nanotube structures were calculated using Xplor-NIH based on experimental restraints on interatomic distances from solid-state NMR and nanotube radius from TEM. The monomer structures have not been aligned with respect to one another, with the observed spread being primarily due to small angle (< ~4°) in-plane rotations of entire monolayer rings. (Middle) The same 20 lowest-energy structures aligned with respect to the central NDI moiety. The heavy atom coordinates for this structural ensemble show RMSDs ranging from 0.2 to 0.4 Å relative to the lowest-energy conformer shown at the bottom of the panel. (b) Top view of the central monolayer ring extracted from the lowest-energy nanotube structure showing the details of the assembly of 52 NDI-Lys monomers into the ring structure. (c) Lowest-energy nanotube structure showing the details of the nanotube assembly via the stacking of multiple monolayer rings. The analysis of sets of representative monomers from the three central rings for the entire ensemble of 20 lowest-energy structures reveals average distances between nearest-neighbor NDI chromophores of 6.0 ± 0.1 Å within the same ring and 5.1 ± 0.2 Å between adjacent rings and an average NDI plane tilt of 25.0 ± 0.5°. The NDI plane distances and tilts were obtained using the aromatic carbon atoms located in the central part of the NDI moiety. (d) Space-filling surface model of an extended 20-ring nanotube constructed by propagating the central three rings from the lowest-energy nanotube structure (panel b) according to the ~5 Å inter-ring distance determined for the nanotubes (panel c). The nanotube outer diameter and wall-thickness derived from the structural model are indicated. (e), Comparison of experimental[29] and calculated XRD patterns for NDI-Lys nanotubes. The calculated pattern was generated as described in the Supporting Information and corresponds to the average for the ensemble of 20 lowest-energy nanotube structures. (f,g) Representative TEM image of NDI-Lys nanotubes used in this study, negatively stained with uranyl acetate (panel f) as described previously,[29] with close-up views indicating the approximate diameters of an individual nanotube and monolayer ring (panel g). (h) Histogram showing the distribution of NDI-Lys nanotube outer diameters obtained from a quantitative analysis of a large set of TEM images using the ImageJ software (http://rsb.info.nih.gov/ij). The average nanotube outer diameter was found to be 12.1 ± 0.3 nm.

of the relatively narrow distribution of nanotube widths (Figure 2h).

With the number of NDI-Lys monomers per ring established, we proceeded with the final structure calculations for nanotubes

DOI: 10.1021/acs.jpcc.5b03398
J. Phys. Chem. C 2015, 119, 13948−13956

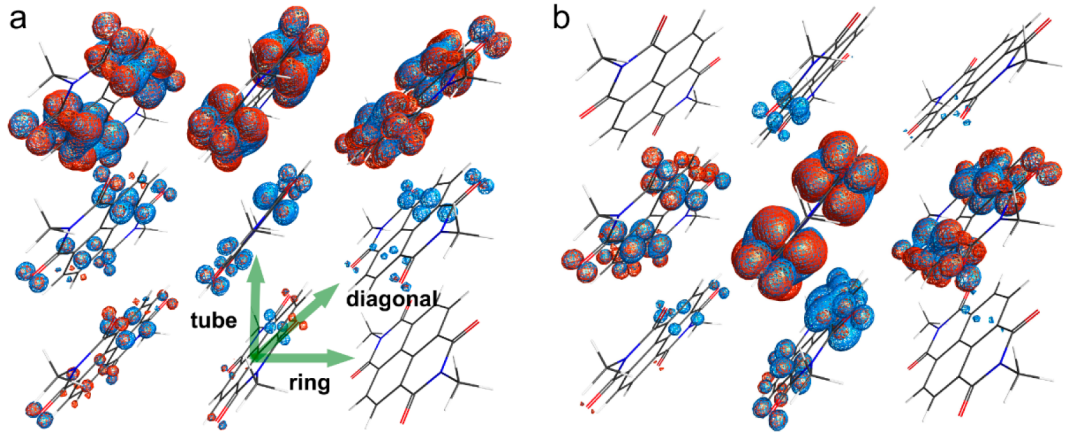

Figure 3. Quantum chemical calculation of excited-state wave functions. (a) Attachment density (in red) and detachment density (in blue) for the lowest-energy bright state of a nine-NDI subunit of the nanotube corresponding to the structural model in Figure 2c, with the tube, ring, and diagonal directions indicated. Delocalization along the ring axis is evident. (b) Attachment and detachment densities for an excited state, which exhibits delocalization along both the ring and tube directions and lies just 0.2 eV below the bright state.

composed of seven rings as described in the Methods section. Figure 2a shows the 20 lowest-energy structures for a representative NDI-Lys monomer extracted from the ensemble of corresponding nanotube structures (Figure S2 of the Supporting Information). The minor spread in the unaligned monomer structures is caused primarily by small angle (<~4°) in-plane rotations of entire monolayer rings with respect to each other rather than differences in the local conformations of individual NDI-Lys monomers in the ensemble. Consistent with the abundance of structurally informative solid-state NMR distances, the conformation of the inner K1 lysine headgroup is established with particularly high precision. On the other hand, the relatively flexible K2 moiety depicted in the structural model corresponds to one of the probable low-energy topologies that this headgroup can adopt that satisfies the experimental $^{13}C'-^{13}C\varepsilon$ distance restraint while minimizing steric clashes with the neighboring NDI-Lys molecules. Panels b and c of Figure 2 show the details of the assembly of NDI-Lys monomers into monolayer rings and the nanotube structure formed by the stacking of multiple rings, respectively, and Figure 2d shows a space-filling surface model for a nanotube containing 20 monolayer rings constructed by propagating the central three rings from the lowest-energy structure.

In the final nanotube structural model in Figure 2, the individual monolayer rings are found to consist of 52 NDI-Lys molecules having their NDI planes tilted by ca. 25° with respect to the ring normal and are held together by a combination of cooperative electrostatic NH_3^+ and COO^- salt-bridge and $\pi-\pi$ stacking interactions that locate adjacent NDI chromophores ~6 Å from each other. The presence of the attractive electrostatic interactions is consistent with the previously demonstrated inability of a methyl ester analogue of NDI-Lys to form higher-order nanostructures of any kind, including isolated monolayer rings and extended nanotubes.[29] The stacking of multiple rings appears to be mediated by additional $\pi-\pi$ interactions between NDI moieties that yield a ~5 Å separation between the chromophores.

The structural model yields a nanotube wall thickness and outer diameter of 2.1 and 12.1 nm, respectively; the latter dimension is in agreement with the average nanotube width of 12.1 ± 0.3 nm determined by TEM (Figure 2h). The ensemble of 20 lowest-energy structures was further used to calculate an XRD pattern for the NDI-Lys nanotube model, and the result compared with the previously recorded experimental pattern[29] (Figure 2e). While the calculated XRD pattern is unable to exactly reproduce the experimental diffraction peak intensities and positions it qualitatively captures the most prominent features including the number of diffraction peaks and their approximate locations, particularly for the larger diffraction angles (2θ > ~10°). This level of agreement appears reasonable considering that (i) the structural model corresponds to an idealized depiction of a small segment of the NDI-Lys nanotube assembly that cannot fully account for the heterogeneity inherent to a macroscopic nanotube hydrogel sample, (ii) the calculated XRD patterns are quite sensitive to the fine details of intermolecular stacking and NDI plane tilt (see Figures S3 and S4 of the Supporting Information), and (iii) the structure calculation procedure did not employ the complete experimental XRD pattern as an active restraint. Most importantly, in addition to the major feature at 2θ = ~15° reporting on the spacing between adjacent NDI-Lys monomers within the ring as discussed above, close inspection of the XRD patterns calculated for a series of test nanotube structural models having different numbers of stacked monolayer rings (Figure S3 in the Supporting Information) and varying NDI plane tilts (Figure S4 in the Supporting Information) reveals that diffraction peaks in the region 2θ = ~18−25° arise from the presence of tilted NDI chromophores combined with the stacking of multiple monolayer rings, which is in agreement with both the nanotube structural model in Figure 2 and the experimental XRD pattern. Finally, in Figure S5 in the Supporting Information, we confirm that the majority of the experimental NMR distances, which were employed as restraints in the structure calculation protocol, agree within experimental error with the corresponding distances in the final nanotube structural model.

Electronic Structure Calculations for the NDI-Lys Nanotube. The NDI-Lys nanotube structural model provides an opportunity to probe how excitation energy migrates through this assembly. First-order exciton couplings between the long-axis polarized transitions of adjacent pairs of NDI chromophores were calculated based on transition densities obtained from time-dependent density functional theory (TDDFT) with a polarizable continuum model (B3LYP/6-31G*/C-PCM), as described in the Methods section.[35,36] The NDI pairs were positioned according to the periodic molecular arrangement determined in the structural model of Figure 2, with lysine side

DOI: 10.1021/acs.jpcc.5b03398
J. Phys. Chem. C 2015, 119, 13948−13956

chains replaced by methyl groups. The largest coupling value (376 cm^{-1}) is found along the tube axis, whereas couplings of 228 and 175 cm^{-1} are obtained for the ring and diagonal directions, respectively (see Figure 3 for the definition of tube, ring, and diagonal coordinates). We then used these couplings, in conjunction with Fermi's golden rule, to calculate energy-transfer rates using an incoherent transfer model.[37] The Franck–Condon weighted density of states was evaluated in terms of normalized absorption and fluorescence spectra for the NDI-Lys monomer,[29] and hopping times of 0.21, 0.58, and 0.99 ps were obtained along the tube, ring, and diagonal directions, respectively. In the Discussion section, we connect these theoretical hopping times to time-resolved fluorescence anisotropy (TRFA) measurements, which indeed suggest a sub-picosecond time scale for energy transfer.

In addition, we performed TDDFT/3-21G* calculations on a nine-NDI subunit of the nanotube structural model, corresponding to three NDI chromophores from each of three adjacent monolayer rings. As can be inferred from the attachment and detachment densities[38] shown in Figure 3a, the first optically bright excited state is mainly localized along the ring direction. Natural transition orbitals[39] (NTOs) for this excitation (Figure S7 in the Supporting Information) reveal that this state can be conceptualized as a linear combination of $\pi\pi^*$ excitations on three different monomer units arranged along the ring direction, with a small amount of delocalization along the nanotube axis. However, a dense manifold of optically dark states exists just below the bright state, and given the large excitonic couplings in all three directions, it is not difficult to find excited states that are strongly delocalized along the nanotube axis. One such state, which lies only 0.2 eV below the bright state, is depicted in Figure 3b. On the basis of this dense manifold of excited states (26 states located within 0.5 eV below the bright state in the nine-NDI model, and likely assuming a band structure in the full nanotube) we expect rapid energy migration out of the bright state in all directions.

DISCUSSION

The structural model for NDI-Lys nanotubes determined based on experimental restraints from solid-state NMR, TEM, and XRD reveals a tightly coupled 2D-crystal-like network of NDI chromophores. Interestingly, this structure possesses some of the key features of cyclic arrays of light-harvesting complexes of bacteriochlorophyll[12] as well as three-dimensional crystals of alkyl NDI derivatives (Figure S6 in the Supporting Information).

In an ordered molecular aggregate with no system–environment interactions, excitations may be completely delocalized over the entire aggregate. However, disorder such as local variations in the structure as well as fluctuations in the surrounding medium tend to localize excitation energy onto a small portion of the aggregate. The extent to which an electronically excited state is delocalized depends on the relative magnitudes of the excitonic coupling as compared to variations in the on-site excitation energies that are the result of structural heterogeneity. If these variations are comparable to the coupling strength, the excitations will localize.[12,40−42] Excitonic couplings determined above for NDI are comparable to the values of 250–400 cm^{-1} that have been estimated for the well-studied BChl pigments in the ring-like structure of bacterial light-harvesting complexes.[12,30,31,43,44] In the LH2 complex, the static disorder in the on-site energies is ∼200 cm^{-1}, comparable to the excitonic coupling, suggesting that the excitation energy is not delocalized over the entire ring.[12,41,42,45] The disorder in the nanotube is much larger than that in LH2, as may be inferred from the absorption spectrum.[29] Thus, we anticipate a fairly localized excitation in the nanotube, which is consistent with the wave functions computed for the nine-NDI unit model (see Figure 3). On the other hand, the excitation is certainly delocalized across more than two monomer units, so it is unclear whether potential energy scans of just two monomer units, which have successfully explained certain aspects of the spectroscopy of *H*-aggregates of perylene diimide,[46−48] would be efficacious here.

The electronic properties of π-conjugated materials are highly sensitive to the details of intermolecular packing of the constituent chromophores, as these interactions determine the domain structure, extent of $\pi-\pi$ overlap, and interfacial spacings that are responsible for the efficiency of energy transfer, charge separation, and carrier mobility in devices. To provide ideas for rational design of novel materials, it is necessary to understand the nature and distance dependence of the excitonic couplings. The distance dependence of the couplings between a pair of NDI chromophores along coordinates corresponding to the three axes of the nanotube labeled in Figure 3 is shown in Figure S8a in the Supporting Information. Interestingly, the coupling along the diagonal direction, which displays the least extensive $\pi-\pi$ overlap between the NDI chromophores, is found to exhibit a much different dependence at short distances as compared to the tube or ring directions. This finding deviates from the widely used Förster theory based on the dipole coupling approximation,[49] which predicts identical distance dependence along the three nanotube axes. Given that the structural parameters of the nanotube are well within the short-range part of the coupling profiles, it follows that the couplings not only are determined by the magnitudes and relative orientations of the chromophore transition dipoles but also are sensitive to orbital overlap and higher-order multipole effects.[50] The latter highlights the important role that $\pi-\pi$ contacts play in modulating the excitonic couplings and underscores the need for high-level theoretical calculations.

A key feature of the NDI-Lys nanotubes is the rapid fluorescence depolarization observed in time-resolved fluorescence anisotropy experiments, for which depolarization time constants of 16.6 ps (major component) and 8.7 ps (minor component) have been measured at 410 nm.[29] Given that this wavelength corresponds to NDI-Lys monomer emission, these decay times are likely to primarily correspond to energy transfer via a hopping mechanism between monomers. As discussed in detail in the Supporting Information, a simple hopping model for a ring of identical chromophores (Figure 2b) can be used to relate the measured depolarization time to the hopping time[42] provided that the angle between their transition dipoles is known. With this information obtained from the nanotube structural model, the experimentally measured depolarization times equate to hopping (i.e., energy transfer) times on the order of 0.5–1 ps. Interestingly, the information about exciton dynamics extracted from TRFA experiments is consistent with predictions of the energy-transfer rate based on electronic structure calculations in conjunction with an exciton coupling model (Figure S8b in the Supporting Information), which indicate sub-picosecond energy transfer along all three directions of the nanotube (ring, diagonal, and tube, as defined in Figure 3a) as discussed in the Results section. Perhaps more importantly, analysis of the distance dependence of the energy-transfer rates reveals that there is a range of structural parameters (∼4–6 Å in the ring tangent and tube directions, and <8 Å in the diagonal tangent direction) for which such sub-picosecond energy transfer

DOI: 10.1021/acs.jpcc.5b03398
J. Phys. Chem. C 2015, 119, 13948−13956

is predicted to occur. This suggests that other materials of this type, exhibiting extremely fast excited-state energy transfer, may be designed via molecular self-assembly.

This hypothesis is emboldened by additional quantum-chemical calculations on a nine-unit model in which the monomers are displaced by 1 Å along both the ring and tube directions (see Figures S9 and S10 and accompanying discussion in the Supporting Information). This perturbed structural model lies near the edge of the parameter space where predicted energy-transfer rate constants are consistent with experimental results (Figure S8b in the Supporting Information). Nevertheless, excitonic delocalization persists, though it is qualitatively different because of changes in the relative coupling constants in the ring, tube, and diagonal directions. Furthermore, these calculations suggest that the perturbed structure lies close to the point where the initially formed excitation would be localized on a single NDI chromophore.

The ability to manipulate the structure of nanoscale architectures with high precision would greatly enable the design and discovery of materials with new or optimal properties. The resemblance of the nanotube structural model described in this work to the cyclic arrays of π-stacked BChl molecules in bacterial light-harvesting complexes is noteworthy. The strong correlation of the coupling strengths with the interchromophore $\pi-\pi$ contacts in the nanotube, an observation similarly reported for natural light harvesting complexes,[9] indicates that controlling these interactions is an important design element for optoelectronic materials. Molecular aggregation strongly influences the nature of these $\pi-\pi$ contacts, but modulating these interactions with the precision necessary to optimize performance is exceptionally challenging and often discovered by trial and error. The structural model determined here for the NDI-Lys nanotubes may serve as a platform from which to build structural variants that explore how atomic-level perturbations of the $\pi-\pi$ contacts impact the corresponding optoelectronic properties. In this context it is also important to note that the solid-state NMR based structural analysis approach described here for the NDI-Lys nanotubes is expected to be applicable to other molecules[51] that can be appropriately isotope labeled and assembled into ordered architectures. Finally, until significant advances in the precision of nanoscale synthesis are realized, detailed structural characterization coupled with theory and simulation are expected to play important roles in guiding the design of self-assembled materials to enhance performance and discover novel phenomena.

METHODS

Sample Preparation. The synthesis of NDI-Lys containing natural abundance, ^{13}C-, ^{15}N- or ^{13}C,^{15}N-labeled lysine headgroups was carried out as described previously.[29] Two types of nanotube hydrogels were used for the solid-state NMR analysis: diluted (prepared from a physical mixture ^{13}C,^{15}N-NDI-Lys and natural abundance NDI-Lys in a 15:85 molar ratio) and mixed (prepared from a physical mixture of ^{13}C-NDI-Lys and ^{15}N-NDI-Lys in a 1:1 molar ratio). The nanotubes were prepared by dissolving the appropriate NDI-Lys precursors in trifluoroethanol (TFE) with 2% trifluoroacetic acid, followed by air drying to remove the TFE, dissolution in HPLC grade water at a concentration of 10 mg/mL, brief sonication, and incubation for 24 h at ambient temperature. The nanotubes were routinely characterized by TEM as described previously,[29] and for each NMR sample, ~20 mg of total material was packed into a 3.2 mm zirconia rotor (Agilent Technologies) by ultracentrifugation.

NMR Spectroscopy. NMR spectra were recorded on a 500 MHz Varian spectrometer equipped with triple-resonance 3.2 mm T3 and BioMAS probes. The MAS rates ranged between ~8−11 kHz ± 5 Hz for the different experiments, and the sample temperature was regulated at ~10 °C. Spectra were processed using NMRPipe[52] and analyzed using nmrglue.[53] The intramolecular $^{13}C-^{13}C$ and $^{13}C-^{15}N$ distances were determined for the diluted nanotube sample using the rotational resonance width[33] and z-filtered TEDOR experiments,[32] respectively, while the intermolecular $^{13}C-^{15}N$ distances were probed using the mixed nanotube sample and band-selective TEDOR,[32] as described in detail in the Supporting Information.

Structure Calculations. The nanotube structure calculations were carried out using simulated annealing molecular dynamics in Xplor-NIH[54] starting from an initial model composed of seven monolayer rings, with a total of 200 structures generated and the 20 lowest-energy structures used for the subsequent analysis. Each ring was made up of 52 NDI-Lys monomers with both lysine headgroups initially in a fully extended conformation and the NDI moiety oriented with its normal perpendicular to the long axis of the nanotube (i.e., angle $\varphi = 0°$ in Figure S4a in the Supporting Information). Seven rings were used to represent an elongated nanotube and minimize the influence of edge effects on the molecular conformation of the central rings while keeping the calculation times reasonable. The inclusion of 52 NDI-Lys monomers per ring in the final structure calculations was based on a systematic evaluation of the consistency with experimental XRD and NMR intramolecular distance data for preliminary nanotube structural models calculated with different numbers of monomers as described in detail in the Results section and Figure S1 in the Supporting Information.

The structure calculations, which are described in detail in the Supporting Information, included restraints on the monolayer ring diameter based on TEM measurements of the nanotube width, noncrystallographic symmetry restraints to ensure that all the NDI-Lys monomers have near identical conformations consistent with the observation of single sets of resonances for the lysine headgroups in solid-state NMR spectra, as well as standard energy terms corresponding to intramolecular $^{13}C-^{13}C$ and $^{13}C-^{15}N$ distances. In addition, the calculation protocol included restraints on intermolecular K1C′−Nα and K1Cε−Nζ distances determined using the mixed nanotube sample (cf., Table 1), taken to report on the separation between neighboring NDI-Lys molecules located within a monolayer ring and between adjacent monolayer rings, respectively, as discussed below. The intermolecular K1C′−Nα distance of 3.7 Å is highly indicative of an NH_3^+ and COO^- salt-bridge.[55] The fact that a methyl ester analogue of NDI-Lys does not assemble into monolayer rings or any other higher-order nanostructures[29] strongly suggests that multiple cooperative $NH_3^+-COO^-$ ion-pair interactions involving the lysine headgroup located on the inner surface of the nanotube are responsible for stabilizing the monolayer ring structures. To ensure a proper directionality of these electrostatic interactions, this restraint was further supplemented by restraining the distance between the proton and oxygen atoms of the NH_3^+ and COO^- groups, respectively, to be less than 2.5 Å. For the intermolecular K1Cε−Nζ interaction, the band-selective TEDOR trajectory (Figure 1g) is dominated by a shortest $^{13}C-^{15}N$ spin-pair separation of 5.0 Å. This relatively short distance cannot arise from neighboring NDI-Lys molecules within a monolayer ring because it is incompatible with the ~6 Å intraring spacing for NDI chromophores—supported by both

DOI: 10.1021/acs.jpcc.5b03398
J. Phys. Chem. C 2015, 119, 13948−13956

experimental XRD and intermolecular K1C′−Nα distance data—and thus is taken to correspond to the distance between nearest-neighbor NDI-Lys molecules located in adjacent rings. Note that the experimental intermolecular K1Cα−Nα distance, which could not be readily assigned to an intraring or inter-ring spacing between NDI-Lys monomers, was not included as an active restraint in the calculations but rather utilized subsequently to validate the nanotube structural models.

Quantum Chemical Calculations. Excitation energies, orbitals, and transition densities were obtained from TDDFT calculations performed using a locally modified version of Q-Chem.[56,57] As described in the Supporting Information, monomer transition densities (B3LYP/6-31G*/C-PCM) were used to compute pairwise excitonic couplings using established formalism. To avoid spurious charge transfer in calculations on the nine-NDI unit model, a long-range corrected functional (LRC-ωPBE) was used, which was tuned to afford proper long-range behavior of the exchange-correlation potential. The qualitative nature of the excitations was characterized in terms of attachment and detachment densities[38] and NTOs.[39]

■ ASSOCIATED CONTENT

Supporting Information

Additional details of NMR data acquisition and analysis, calculation of XRD patterns, structure and quantum chemical calculations, and supporting figures. The Supporting Information is available free of charge on the ACS Publications website at DOI: 10.1021/acs.jpcc.5b03398.

■ AUTHOR INFORMATION

Corresponding Authors

*E-mail: herbert@chemistry.ohio-state.edu.
*E-mail: parquett@chemistry.ohio-state.edu.
*E-mail: jaroniec@chemistry.ohio-state.edu.

Present Addresses

[‖]M.G.: Dow Chemical Company, Freeport, TX 77541.
[¶]S.P.: CEA, INAC, F-38000 Grenoble, France.
[#]H.S.: Dow AgroSciences LLC, Indianapolis, IN 46268.

Author Contributions

[§]M.G. and S.P.: These authors contributed equally.

Notes

The authors declare no competing financial interest.

■ ACKNOWLEDGMENTS

This research was supported by grants from the National Science Foundation (MCB-1243461 to C.P.J., CHE-0748448 to J.M.H., and CHE-1412295 to J.R.P.), the National Institutes of Health (R01GM094357 to C.P.J.), the Camille and Henry Dreyfus Foundation (Camille Dreyfus Teacher-Scholar Award to C.P.J. and J.M.H), and the Alfred P. Sloan Foundation (Research Fellowship to J.M.H.). C.D.S. was supported by the NIH Intramural Research Program of the Center for Information Technology.

■ REFERENCES

(1) Sirringhaus, H.; Brown, P. J.; Friend, R. H.; Nielsen, M. M.; Bechgaard, K.; Langeveld-Voss, B. M. W.; Spiering, A. J. H.; Janssen, R. A. J.; Meijer, E. W.; Herwig, P.; et al. Two-Dimensional Charge Transport in Self-Organized, High-Mobility Conjugated Polymers. *Nature* **1999**, *401*, 685−688.

(2) Schwartz, B. J. Conjugated Polymers as Molecular Materials: How Chain Conformation and Film Morphology Influence Energy Transfer and Interchain Interactions. *Annu. Rev. Phys. Chem.* **2003**, *54*, 141−172.

(3) Yamamoto, Y.; Fukushima, T.; Suna, Y.; Ishii, N.; Saeki, A.; Seki, S.; Tagawa, S.; Taniguchi, M.; Kawai, T.; Aida, T. Photoconductive Coaxial Nanotubes of Molecularly Connected Electron Donor and Acceptor Layers. *Science* **2006**, *314*, 1761−1764.

(4) Lu, Z. H.; Lockwood, D. J.; Baribeau, J. M. Quantum Confinement and Light-Emission in SiO_2/Si Superlattices. *Nature* **1995**, *378*, 258−260.

(5) Alivisatos, A. P. Semiconductor Clusters, Nanocrystals, and Quantum Dots. *Science* **1996**, *271*, 933−937.

(6) Zhang, Q.; Uchaker, E.; Candelaria, S. L.; Cao, G. Nanomaterials for Energy Conversion and Storage. *Chem. Soc. Rev.* **2013**, *42*, 3127−3171.

(7) Baxter, J.; Bian, Z. X.; Chen, G.; Danielson, D.; Dresselhaus, M. S.; Fedorov, A. G.; Fisher, T. S.; Jones, C. W.; Maginn, E.; Kortshagen, U.; et al. Nanoscale Design to Enable the Revolution in Renewable Energy. *Energy Environ. Sci.* **2009**, *2*, 559−588.

(8) Marek, P. L.; Hahn, H.; Balaban, T. S. On the Way to Biomimetic Dye Aggregate Solar Cells. *Energy Environ. Sci.* **2011**, *4*, 2366−2378.

(9) Scholes, G. D.; Fleming, G. R.; Olaya-Castro, A.; van Grondelle, R. Lessons from Nature About Solar Light Harvesting. *Nat. Chem.* **2011**, *3*, 763−774.

(10) McQuade, D. T.; Pullen, A. E.; Swager, T. M. Conjugated Polymer-Based Chemical Sensors. *Chem. Rev. (Washington, DC, U.S.)* **2000**, *100*, 2537−2574.

(11) Aratani, N.; Kim, D.; Osuka, A. Discrete Cyclic Porphyrin Arrays as Artificial Light-Harvesting Antenna. *Acc. Chem. Res.* **2009**, *42*, 1922−1934.

(12) Cogdell, R. J.; Gall, A.; Kohler, J. The Architecture and Function of the Light-Harvesting Apparatus of Purple Bacteria: From Single Molecules to in Vivo Membranes. *Q. Rev. Biophys.* **2006**, *39*, 227−324.

(13) Harel, E.; Engel, G. S. Quantum Coherence Spectroscopy Reveals Complex Dynamics in Bacterial Light-Harvesting Complex 2 (LH2). *Proc. Natl. Acad. Sci. U.S.A.* **2012**, *109*, 706−711.

(14) Whitesides, G. M.; Mathias, J. P.; Seto, C. T. Molecular Self-Assembly and Nanochemistry: A Chemical Strategy for the Synthesis of Nanostructures. *Science* **1991**, *254*, 1312−1319.

(15) Grzybowski, B. A.; Wilmer, C. E.; Kim, J.; Browne, K. P.; Bishop, K. J. M. Self-Assembly: From Crystals to Cells. *Soft Matter* **2009**, *5*, 1110−1128.

(16) Kaiser, T. E.; Wang, H.; Stepanenko, V.; Wurthner, F. Supramolecular Construction of Fluorescent J-Aggregates Based on Hydrogen-Bonded Perylene Dyes. *Angew. Chem., Int. Ed.* **2007**, *46*, 5541−5544.

(17) Frischmann, P. D.; Mahata, K.; Wurthner, F. Powering the Future of Molecular Artificial Photosynthesis with Light-Harvesting Metallosupramolecular Dye Assemblies. *Chem. Soc. Rev.* **2013**, *42*, 1847−1870.

(18) Percec, V.; Dulcey, A. E.; Balagurusamy, V. S.; Miura, Y.; Smidrkal, J.; Peterca, M.; Nummelin, S.; Edlund, U.; Hudson, S. D.; Heiney, P. A.; et al. Self-Assembly of Amphiphilic Dendritic Dipeptides into Helical Pores. *Nature* **2004**, *430*, 764−768.

(19) Pandit, A.; Ocakoglu, K.; Buda, F.; van Marle, T.; Holzwarth, A. R.; de Groot, H. J. Structure Determination of a Bio-Inspired Self-Assembled Light-Harvesting Antenna by Solid-State NMR and Molecular Modeling. *J. Phys. Chem. B* **2013**, *117*, 11292−11298.

(20) Lorieau, J. L.; Day, L. A.; McDermott, A. E. Conformational Dynamics of an Intact Virus: Order Parameters for the Coat Protein of Pf1 Bacteriophage. *Proc. Natl. Acad. Sci. U.S.A.* **2008**, *105*, 10366−10371.

(21) Wasmer, C.; Lange, A.; Van Melckebeke, H.; Siemer, A. B.; Riek, R.; Meier, B. H. Amyloid Fibrils of the Het-S(218−289) Prion Form a β Solenoid with a Triangular Hydrophobic Core. *Science* **2008**, *319*, 1523−1526.

(22) Loquet, A.; Sgourakis, N. G.; Gupta, R.; Giller, K.; Riedel, D.; Goosmann, C.; Griesinger, C.; Kolbe, M.; Baker, D.; Becker, S.; et al.

DOI: 10.1021/acs.jpcc.5b03398
J. Phys. Chem. C 2015, 119, 13948−13956

Atomic Model of the Type III Secretion System Needle. *Nature* **2012**, *486*, 276−279.
(23) Fitzpatrick, A. W.; Debelouchina, G. T.; Bayro, M. J.; Clare, D. K.; Caporini, M. A.; Bajaj, V. S.; Jaroniec, C. P.; Wang, L.; Ladizhansky, V.; Muller, S. A.; et al. Atomic Structure and Hierarchical Assembly of a Cross-β Amyloid Fibril. *Proc. Natl. Acad. Sci. U.S.A.* **2013**, *110*, 5468−5473.
(24) Lu, J. X.; Qiang, W.; Yau, W. M.; Schwieters, C. D.; Meredith, S. C.; Tycko, R. Molecular Structure of β-Amyloid Fibrils in Alzheimer's Disease Brain Tissue. *Cell* **2013**, *154*, 1257−1268.
(25) Rapp, A.; Schnell, I.; Sebastiani, D.; Brown, S. P.; Percec, V.; Spiess, H. W. Supramolecular Assembly of Dendritic Polymers Elucidated by ^{1}H and ^{13}C Solid-State MAS NMR Spectroscopy. *J. Am. Chem. Soc.* **2003**, *125*, 13284−13297.
(26) Chen, W.; Sun, H. J.; Miyoshi, T. Unique Molecular Dynamics of Structural Elements in an Asymmetric Janus Bisamide Supramolecule Characterized by Solid-State NMR. *J. Phys. Chem. B* **2013**, *117*, 13698−13709.
(27) Wu, Y. C.; Leowanawat, P.; Sun, H. J.; Partridge, B. E.; Peterca, M.; Graf, R.; Spiess, H. W.; Zeng, X.; Ungar, G.; Hsu, C. S.; et al. Complex Columnar Hexagonal Polymorphism in Supramolecular Assemblies of a Semifluorinated Electron-Accepting Naphthalene Bisimide. *J. Am. Chem. Soc.* **2015**, *137*, 807−819.
(28) Hansen, M. R.; Graf, R.; Spiess, H. W. Solid-State NMR in Macromolecular Systems: Insights on How Molecular Entities Move. *Acc. Chem. Res.* **2013**, *46*, 1996−2007.
(29) Shao, H.; Seifert, J.; Romano, N. C.; Gao, M.; Helmus, J. J.; Jaroniec, C. P.; Modarelli, D. A.; Parquette, J. R. Amphiphilic Self-Assembly of an N-Type Nanotube. *Angew. Chem., Int. Ed.* **2010**, *49*, 7688−7691.
(30) Sauer, K.; Cogdell, R. J.; Prince, S. M.; Freer, A.; Isaacs, N. W.; Scheer, H. Structure-Based Calculations of the Optical Spectra of the LH2 Bacteriochlorophyll-Protein Complex from Rhodopseudomonas Acidophila. *Photochem. Photobiol.* **1996**, *64*, 564−576.
(31) Krueger, B. P.; Scholes, G. D.; Fleming, G. R. Calculation of Couplings and Energy-Transfer Pathways between the Pigments of LH2 by the Ab Initio Transition Density Cube Method. *J. Phys. Chem. B* **1998**, *102*, 5378−5386.
(32) Jaroniec, C. P.; Filip, C.; Griffin, R. G. 3D TEDOR NMR Experiments for the Simultaneous Measurement of Multiple Carbon-Nitrogen Distances in Uniformly ^{13}C,^{15}N-Labeled Solids. *J. Am. Chem. Soc.* **2002**, *124*, 10728−10742.
(33) Ramachandran, R.; Ladizhansky, V.; Bajaj, V. S.; Griffin, R. G. ^{13}C-^{13}C Rotational Resonance Width Distance Measurements in Uniformly ^{13}C-Labeled Peptides. *J. Am. Chem. Soc.* **2003**, *125*, 15623−15629.
(34) Helmus, J. J.; Surewicz, K.; Apostol, M. I.; Surewicz, W. K.; Jaroniec, C. P. Intermolecular Alignment in Y145stop Human Prion Protein Amyloid Fibrils Probed by Solid-State NMR Spectroscopy. *J. Am. Chem. Soc.* **2011**, *133*, 13934−13937.
(35) Hsu, C.-P.; Fleming, G. R.; Head-Gordon, M.; Head-Gordon, T. Excitation Energy Transfer in Condensed Media. *J. Chem. Phys.* **2001**, *114*, 3065−3072.
(36) Iozzi, M. F.; Mennucci, B.; Tomasi, J.; Cammi, R. Excitation Energy Transfer (EET) between Molecules in Condensed Matter: A Novel Application of the Polarizable Continuum Model (PCM). *J. Chem. Phys.* **2004**, *120*, 7029−7040.
(37) Dirac, P. A. M. The Quantum Theory of the Emission and Absorption of Radiation. *Proc. R. Soc. London, Ser. A* **1927**, *114*, 243−265.
(38) Head-Gordon, M.; Graña, A. M.; Maurice, D.; White, C. A. Analysis of Electronic Transitions as the Difference of Electron Attachment and Detachment Densities. *J. Phys. Chem.* **1995**, *99*, 14261−14270.
(39) Martin, R. L. Natural Transition Orbitals. *J. Chem. Phys.* **2003**, *118*, 4775−4777.
(40) Fidder, H.; Knoester, J.; Wiersma, D. A. Optical Properties of Disordered Molecular Aggregates: A Numerical Study. *J. Chem. Phys.* **1991**, *95*, 7880−7890.
(41) Leegwater, J. A. Coherent Versus Incoherent Energy Transfer and Trapping in Photosynthetic Antenna Complexes. *J. Phys. Chem.* **1996**, *100*, 14403−14409.
(42) Jimenez, R.; Dikshit, S. N.; Bradforth, S. E.; Fleming, G. R. Electronic Excitation Transfer in the LH2 Complex of Rhodobacter Sphaeroides. *J. Phys. Chem.* **1996**, *100*, 6825−6834.
(43) Monshouwer, R.; van Grondelle, R. Excitations and Excitons in Bacterial Light-Harvesting Complexes. *Biochim. Biophys. Acta* **1996**, *1275*, 70−75.
(44) Scholes, G. D.; Gould, I. R.; Cogdell, R. J.; Fleming, G. R. Ab Initio Molecular Orbital Calculations of Electronic Couplings in the LH2 Bacterial Light-Harvesting Complex of Rps. Acidophila. *J. Phys. Chem. B* **1999**, *103*, 2543−2553.
(45) Alden, R. G.; Johnson, E.; Nagarajan, V.; Parson, W. W.; Law, C. J.; Cogdell, R. G. Calculations of Spectroscopic Properties of the LH2 Bacteriochlorophyll−Protein Antenna Complex from Rhodopseudomonas Acidophila. *J. Phys. Chem. B* **1997**, *101*, 4667−4680.
(46) Fink, R. F.; Seibt, J.; Engel, V.; Renz, M.; Kaupp, M.; Lochbrunner, S.; Zhao, H. M.; Pfister, J.; Wurthner, F.; Engels, B. Exciton Trapping in P-Conjugated Materials: A Quantum-Chemistry-Based Protocol Applied to Perylene Bisimide Dye Aggregates. *J. Am. Chem. Soc.* **2008**, *130*, 12858−12859.
(47) Zhao, H. M.; Pfister, J.; Settels, V.; Renz, M.; Kaupp, M.; Dehm, V. C.; Wurthner, F.; Fink, R. F.; Engels, B. Understanding Ground- and Excited-State Properties of Perylene Tetracarboxylic Acid Bisimide Crystals by Means of Quantum Chemical Computations. *J. Am. Chem. Soc.* **2009**, *131*, 15660−15668.
(48) Settels, V.; Schubert, A.; Tafipolski, M.; Liu, W.; Stehr, V.; Topczak, A. K.; Pflaum, J.; Deibel, C.; Fink, R. F.; Engel, V.; et al. Identification of Ultrafast Relaxation Processes as a Major Reason for Inefficient Exciton Diffusion in Perylene-Based Organic Semiconductors. *J. Am. Chem. Soc.* **2014**, *136*, 9327−9337.
(49) Förster, T. Zwischenmolekulare Energiewanderung Und Fluoreszenz. *Ann. Phys. (Leipzig)* **1948**, *2*, 55−75.
(50) You, Z.-Q.; Hsu, C.-P. Theory and Calculation for the Electronic Coupling in Excitation Energy Transfer. *Int. J. Quantum Chem.* **2014**, *114*, 102−115.
(51) Shao, H.; Gao, M.; Kim, S. H.; Jaroniec, C. P.; Parquette, J. R. Aqueous Self-Assembly of L-Lysine-Based Amphiphiles into 1D N-Type Nanotubes. *Chem.—Eur. J.* **2011**, *17*, 12882−12885.
(52) Delaglio, F.; Grzesiek, S.; Vuister, G. W.; Zhu, G.; Pfeifer, J.; Bax, A. NMRpipe: A Multidimensional Spectral Processing System Based on Unix Pipes. *J. Biomol. NMR* **1995**, *6*, 277−293.
(53) Helmus, J. J.; Jaroniec, C. P. Nmrglue: An Open Source Python Package for the Analysis of Multidimensional NMR Data. *J. Biomol. NMR* **2013**, *55*, 355−367.
(54) Schwieters, C. D.; Kuszewski, J. J.; Tjandra, N.; Clore, G. M. The Xplor-NIH NMR Molecular Structure Determination Package. *J. Magn. Reson.* **2003**, *160*, 65−73.
(55) Barlow, D. J.; Thornton, J. M. Ion-Pairs in Proteins. *J. Mol. Biol.* **1983**, *168*, 867−885.
(56) Krylov, A. I.; Gill, P. M. W. Q-Chem: An Engine for Innovation. *Wiley Interdiscip. Rev.: Comput. Mol. Sci.* **2013**, *3*, 317−325.
(57) Shao, Y.; Gan, Z.; Epifanovsky, E.; Gilbert, A. T. B.; Wormit, M.; Kussmann, J.; Lange, A. W.; Behn, A.; Deng, J.; Feng, X.; et al. Advances in Molecular Quantum Chemistry Contained in the Q-Chem 4 Program Package. *Mol. Phys.* **2015**, *113*, 184−215.

DOI: 10.1021/acs.jpcc.5b03398
J. Phys. Chem. C 2015, 119, 13948−13956